Article

Intramolecular Co-reaction Accelerated Electrochemiluminescence of Polypeptide-biomineralized Gold Nanoclusters for Targeted Detection of Biomarkers

Yue Jia, Shanghua Liu, Yu Du, Lei Yang, Xuejing Liu, Lei Liu, Xiang Ren, Qin Wei, and Huangxian Ju

Anal. Chem., **Just Accepted Manuscript** • DOI: 10.1021/acs.analchem.0c01519 • Publication Date (Web): 10 Jun 2020

Intramolecular Co-reaction Accelerated Electrochemiluminescence of Polypeptide-biomineralized Gold Nanoclusters for Targeted Detection of Biomarkers

Yue Jia[†,#], Shanghua Liu[‡,#], Yu Du[†], Lei Yang[†], Xuejing Liu[†], Lei Liu[†], Xiang Ren[†,*], Qin Wei[†,*], Huangxian Ju[†,§]

[†] Collaborative Innovation Center for Green Chemical Manufacturing and Accurate Detection, Key Laboratory of Interfacial Reaction & Sensing Analysis in Universities of Shandong, School of Chemistry and Chemical Engineering, University of Jinan, Jinan 250022, P. R. China

[‡] School of Chemistry and Chemical Engineering, Shandong University of Technology, Zibo, 255049, P. R. China

[§] State Key Laboratory of Analytical Chemistry for Life Science, Department of Chemistry, Nanjing University, Nanjing 210023, China

Corresponding Author

E-mail: chem_renx@163.com (X. R.); sdjndxwq@163.com (Q.W.)

ABSTRACT: The development of label-free electrochemiluminescence (ECL)-based sensing technology for biomarkers detection has a congenital defect compare with non-competitive sandwich-type biosensor due to the lack of detection antibody conjugated with signal label. Nevertheless, it is still not difficult to realize ultrasensitive analysis benefit from the exploration of efficient sensing substrates and signal transducers. In this work, an innovative sensing system is purposed utilizing Fe_2O_3 nanoarrays (Fe_2O_3 NAs) as well-ordered co-reaction accelerator and polypeptide-biomineralized gold nanoclusters (Au NCs) as signal transducer. Bifunctional peptide ligands of H_2N-MMYYHFRRHL-COOH (MYH-10) is self-designed, it can not only play a role of reductant and coupling reagent for clusters formation using MMYY sequence root in N-terminal, but also act as connection for coupling carriers and immune molecules via HFRRHL region of C-terminal. Additional intramolecular ECL emission between Au NCs and tris(3-aminoethyl)amine (TAEA), all strategies undoubtedly reduces the spatial hindrance of the sensing interface and increases the effectiveness of electron transfer and immune recognition. With CYFRA21-1 as target, the biosensor exhibits linear ECL response in a wide range (10 fg mL^{-1} ~ 100 ng mL^{-1}) and an ultralow detection limit of 1.33 fg mL^{-1} (S/N=3). With convincing experimental data, these innovative strategies will be more eye-catching in peptide-based nanocluster synthesis and expansion of more novel thought for sensing platform fabrication.

With slow division and proliferation, non-small cell lung cancer (NSCLC) is often diagnosed in the middle or late period, causing a low five-year survival rate in clinical practice even after surgery and other interventions.[1] It has been proved that CYFRA21-1, a soluble fragment of cytokeratin 19, exists in the cytoplasm of tumor cells, which can be released into the serum when the tumor cells are necrotic and lytic, and is a major biomarker of NSCLC.[2] Therefore, it will be of great significance for the diagnosis of NSCLC if the rapid and sensitive detection of CYFRA21-1 can be realized.

As a major subject emerging from the interdisciplinary integration of electrochemistry, chemiluminiscence and analytical chemistry, electrochemiluminescence (ECL) sensing technology has attracted extensive attention in the detection of biomarkers or environmental pollutants due to its advantages of low detection limit, low cost, easy integration and chip-ability.[3] The sensitivity of ECL-based immunosensor rest largely with the category of luminophor and the microscopic arrangement of the substrate.[4] For now, using conventional micro-nano materials like graphene oxide and metal organic framework for sensing interface fabrication seems ideal in this respect because a large amount of immune molecules can be captured via their huge porosity or specific surface area.[5, 6] However, the smear of substrate materials on electrode surface by manual operation often requires the use of uniform morphology for batch consistency of sensors control precisely.[7] Different grain size or morphology by one-pot chemical synthesis in the final biosensor is clearly unacceptable for accurate analysis of markers.

There is no denying that 3D nanoarrays is selected as the substrate of biosensors can not only provide a larger specific surface area for immobilizing immune molecules on conductive interface, but also significantly accelerate

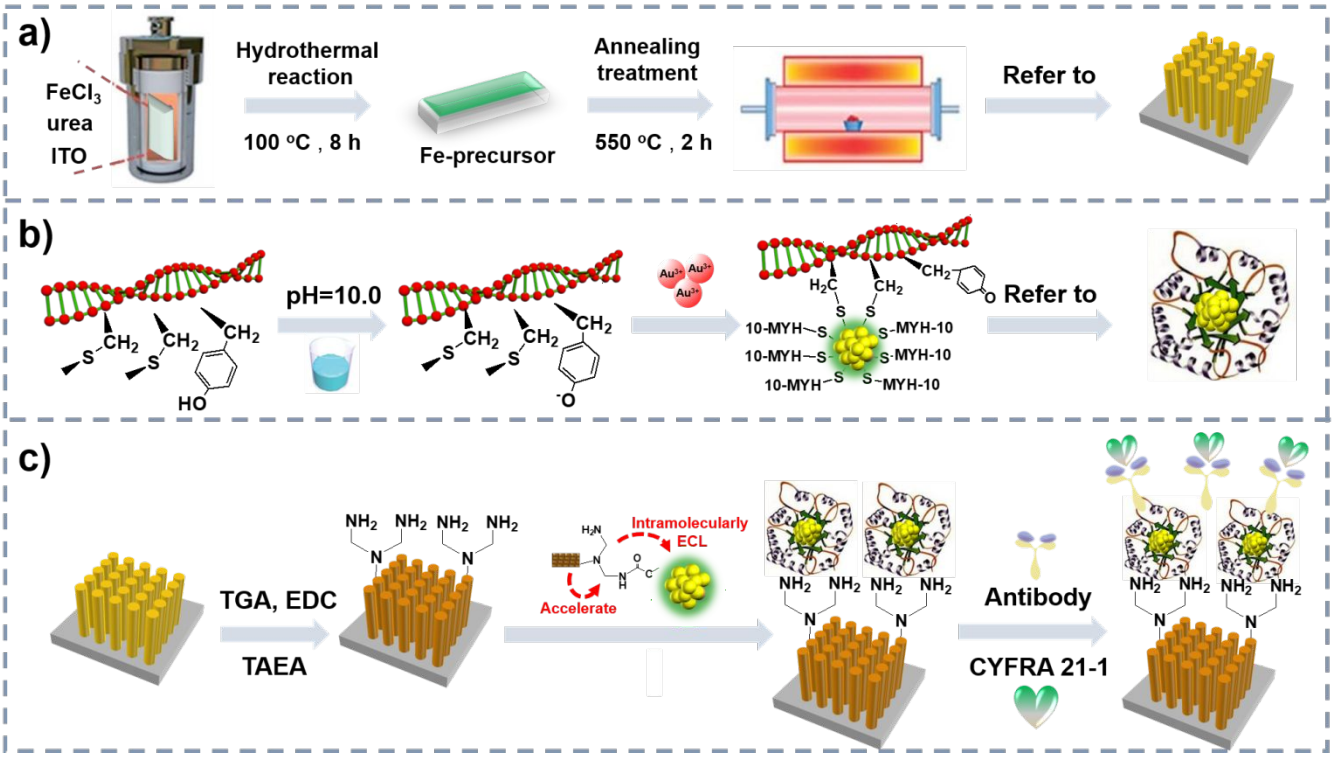

Scheme 1. The synthesis routes of Fe_2O_3 NAs (a) and Au NCs (b). Schematic diagrams showing fabrication of the ECL biosensor (c).

electrochemical process between signal label and electrolyte due to the improved electron-transport along the ordered array structure.[8, 9] As one of the most explored semiconductor oxide, ferric oxide nanoarrays (Fe_2O_3 NAs) have been utilized in photoelectrochemistry catalyzing because of their easily regulated bandgap and excellent redox reversibility of iron ions and ferrous ions.[10, 11] Inspired by this, the expansion of Fe_2O_3 NAs to ECL-based biosensor as both substrate and co-reaction accelerator seems to be feasible. With a sufficient dense of oriented nanoarrays, all the exposed parts become effective for ECL emission enhancement. Meanwhile, it could be electrochemically induced to accelerate the radical reaction by injecting holes into the highest occupied coreactant molecular orbital to excite more high-energy of luminophor.[12] Nevertheless, such topic related to Fe_2O_3 NAs is rarely reported, and the reason lies in the lack of matched ECL luminophor and innovative sensing strategy.

The development of co-reaction-type ECL system to biosensor at the core of care aims at replacing complex annihilation mechanisms, which needs to provide repeated alternating potential.[13, 14] That poses a major challenge to the fabrication of liquid-solid critical surface due to the intrinsic complex luminescence mechanism involving mass transport and ET dynamics of abundant radical intermediates electrogenerated.[15, 16] The intramolecular ECL proposed by Zhou et al undoubtedly breaks this bottleneck by binding the coreactant and luminophor masses to the electrode surface.[17] With a sufficient concision of electron transport, the radical ions can be quickly activated and used for the generation of high-energy-state intermediates to complete photon release root in free radical redox reaction.

Currently, although conventional electroluminescent, for instance, ruthenium (III) complexes, luminol and its derivatives are chosen to fabricate biosensor yield satisfactory results, it is difficult to form bioconjugate with immune molecule in the absence of carriers due to their negligible molecular dimension.[5, 18] Recent, semiconductor quantum dots with remarkable quantum scale effect and surface effect have become the more promising signal label.[19] However, their high redox potential limit their application in immunoassay, since the secondary structures of protein will occur irreversible damage when the electrochemical scanning potential is more than 1.0 V or less than -1.0 V.[20] Therefore, the issue of molecular immobilization and biocompatibility should be considered in the selection of ECL emitters.

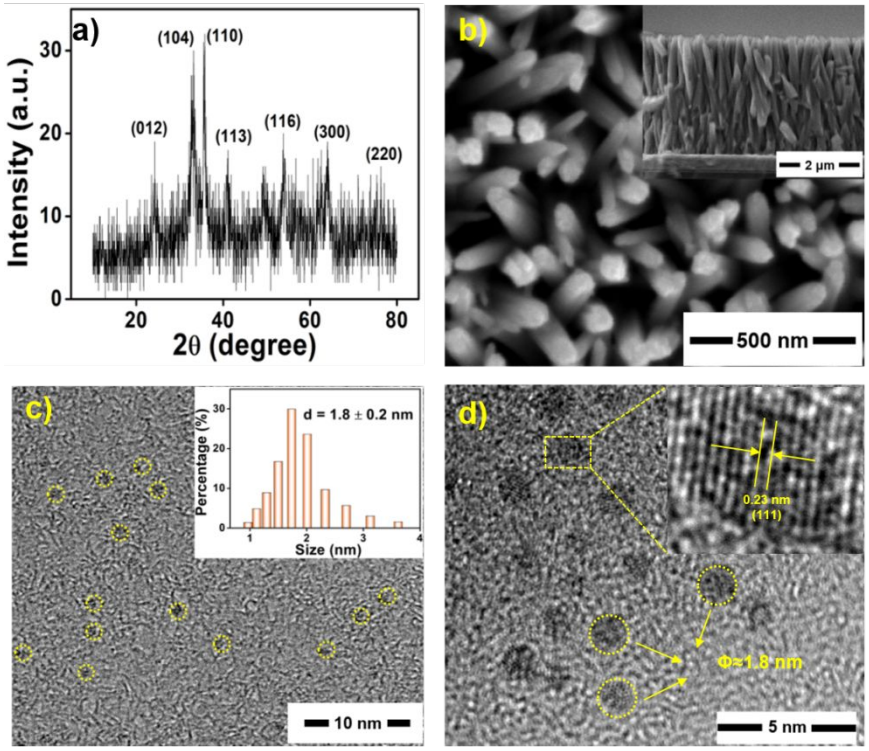

Figure 1. XRD pattern (a), SEM planform and front view image (b and its inset) of Fe_2O_3 NAs. HRTEM images of the Au NCs with 1 0 nm scale (c) and 5 nm scale (d). The inset of part c and d correspond to the size distribution and lattice fringe of Au NCs, respectively.

Gold nanoclusters (Au NCs), a novel type of signal carrier, has been widely used in multiple fields of imaging in vivo, biosensing, drug transfer and photothermal therapy due to its unique optical and electrical properties.[17, 21, 22] To one's excitement, the anodic ECL signal of Au NCs in the presence of tris(3-aminoethyl)amine (TAEA) have been observed by Zhou et al in 2018.[17] But, it is difficult to control the product size using bovine serum albumin (BSA) as template owing to their peptide are diversely different in composition and contain embedded random and inactive amino acid sequences.[23] The versatility of Au NCs is due in large part to their property of size-tunable luminescence which can be varied via quantum size effect, by adjusting the dosage, reaction temperature and pH of the reductant.[24] Instead of stimulating reducing agents, a "top-down" approach is established for Au NCs synthesis employing protein, nucleic acid, peptide, etc. biochemical reagents.[25] Similar to conventional approaches, the synthesis of Au NCs by biochemical reagents requires two basic competencies, i.e., reduction property for Au^0 formation and complexing property for the Au^0 coupling.[26] However, it is well known that not all amino acids (the basic unit of protein) can perform the reductive role unless they are equipped N-heterocyclic or phenolic hydroxyl groups with sp^2 hybridization like proline, tryptophan and tyrosine.[27] Therefore, the strategy of using macromolecular proteins as templates does not hold much prospect. But peptides that have been confirmed through the opposite "bottom-top" approach is useful for the exploitation of thinking for Au NCs preparation.[23] So we can explore a diverse counterplan, where the various required functionalities of a peptide may be assembled from the basic unit of protein in a principled way for Au NCs synthesis and other needs, for instance, surface charge, functional group and targeting.

To better expound the advantages of peptide-based synthesis, a self-designed polypeptide which includes synthetic domain A (MMYY) of Au NCs and specific recognition domain B (HFRRHL) of immunoglobulin G (IgG) is proposed by using MMYYHFRRHL (MYH-10), HFRRHL that immobilizer of antibody, as the connector between Au NCs and immune molecules instead of random immobilization.[28, 29] Furthermore, Fe_2O_3 NAs, which is well-ordered sensing substrate and co-reaction accelerator, shows the best electron-transport capability and catalytic activity when it is grown in situ on indium tin oxide (ITO) electrode. Based on the above, a novel signal amplification-type ECL biosensor is developed utilizing MYH-10-biomineralized Au NCs as signal transducer, TAEA as intramolecular coreactant and Fe_2O_3 NAs as co-reaction accelerator for CYFRA21-1 detection. The development of purposed ECL biosensor is expected to be a potential analytical tool for the early monitoring of squamous carcinoma.

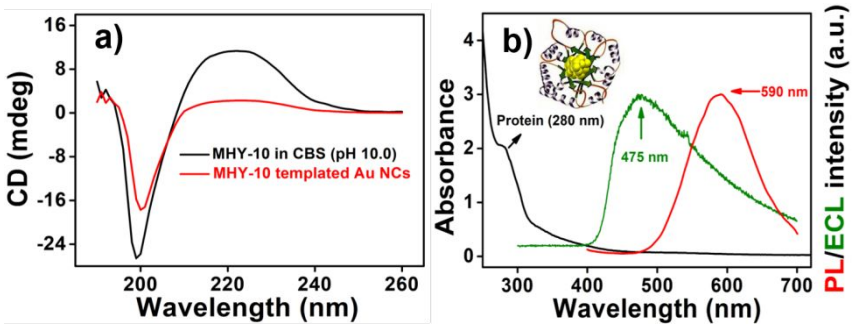

Figure 2. (a) CD spectra of pure MHY-10 in CBS (pH=10.0, black line) and MHY-10-biomineralized Au NCs before dialysis (red curve). (b) UV-vis absorbance (black curve), ECL spectrum (green curve) and PL spectrum (red curve) of Au NCs.

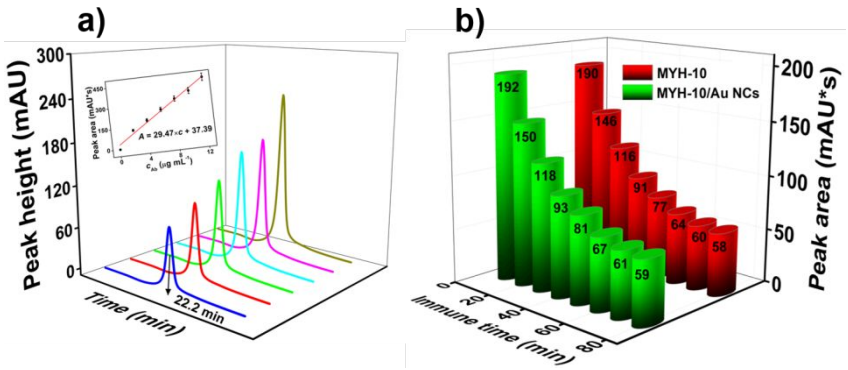

Figure 3. (a) RP-HPLC chromatograms of anti-CYFRA21-1 in diverse concentrations range from 2 μg mL^{-1} to 12 μg mL^{-1} in the retention time of 22.2 min and linear equation between the peak area and the concentrations of anti-CYFRA21-1 (inset); (b) Amount of unconnected anti-CYFRA21-1 (5 μg mL^{-1}) after immunoreaction with pure MYH-10 and MYH-10 templated Au NCs, respectively. Error bars = SD, (n = 3).

EXPERIMENTAL SECTION

Preparation of Fe_2O_3 NAs. The Fe_2O_3 NAs was prepared by hydrothermal synthesis refer to previous literature and the details are shown in Scheme 1a.[30] 0.81 g of hexahydrate ferric chloride ($FeCl_3 \cdot 6H_2O$) and 0.18g of urea ($CO(NH_2)_2$) were dissolved in 40 mL deionized water with vigorous stirring. Then, above mixture was transferred to a 50 mL Teflon-lined stainless-steel autoclave in which a piece of indium tin oxid (ITO)-based glass (1 cm × 2 cm) was immersed into the solution (the conductive interface is down). After heat preservation 100 °C for 8 h, the obtained ITO-covered with Fe-precursor was taken out and washed using deionized water. Finally, the dried Fe-precursor was annealed at 550 °C in air for 2 h to obtain the Fe_2O_3 NAs (the rate of warming is 4 °C per minute).

Preparation of peptide-templated Au NCs. The specific processes of peptide-templated Au NCs was referenced from the previous reports with major modifications.[25] The route is shown in Scheme 1b, MYH-10 (25 mg mL^{-1}, 1 mL) was injected into a 20 mL flask, and the pH was adjusted to 10.0 using the 0.5 M NaOH, aiming at obtain the intermediated phenol oxygen anion. After half an hour, the chloroauric acid hydrated ($HAuCl_4 \cdot 4H_2O$, 25 mM, 5 mL) was injected into the ionized intermediate dropwise. The mixture was sealed and stored at 60 °C for 4 h under slight stirring. In the finally preparation, the flaxen liquid was dialysed for two days using a semipermeable membrane with aperture about 3500Da to empty all OH^-.

Fabrication of the purposed ECL biosensor. The legibly simplified sensing interface of intramolecular ECL emission was fabricated as shown in Scheme 1c. Initially, the Fe_2O_3 NAs was immersed into mercaptoacetic acid (TGA) aqueous solution (3 mM, containing 0.1 M NaCl) to obtain carboxylic product (c-Fe_2O_3).[31] After activization with fresh N-dimethylpropane-1 (EDC, 10 μL, 30 mM), the TAEA (25 μL, 98%) was dropped on ITO to couple with dried c-Fe_2O_3 via amidation. For combining Au NCs, fresh EDC (10 μL, 30 mM) was also dropped into 5 mL of Au NCs to obtain carboxyl-activated Au NCs (a-Au NCs). Then, 6 μL a-Au NCs was dropped c-Fe_2O_3/TAEA electrode is similar to the mechanism of last step. Without any non-specific active sites, the interface of c-Fe_2O_3/TAEA/a-Au NCs can capture antibody specifically via immunoaffinity between HFRRHL hexapeptide and Fc domains of antibody. Finally, the CYFRA21-1 with different concentrations were modified to complete biosensor fabrication. Meanwhile, the electrochemical impedance spectroscopy (EIS) as a conventional analytical tool was employed for demonstrating the feasibility of layering, and the results were shown in Figure S1.

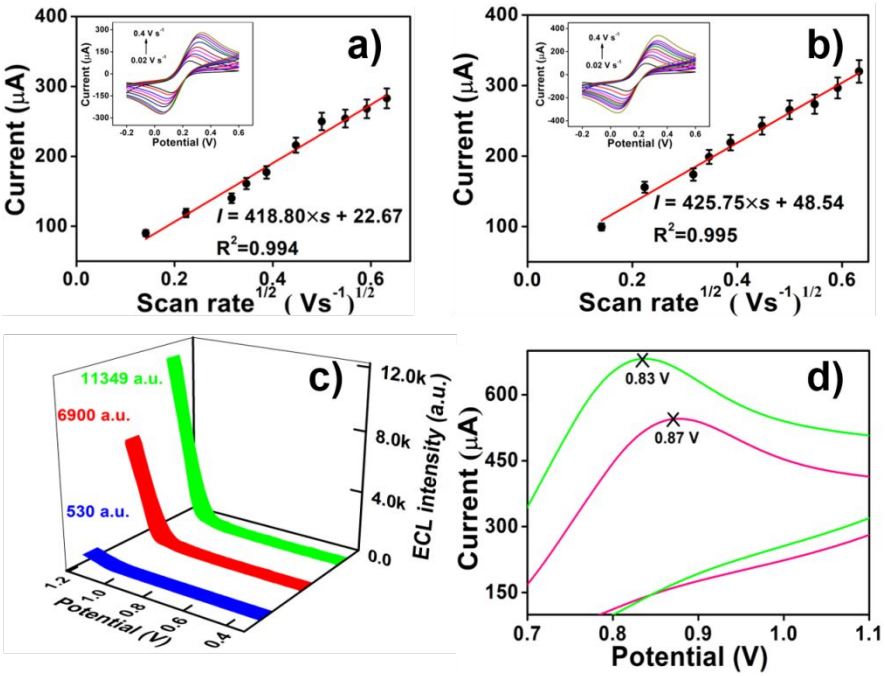

Figure 4. CV curves of pure ITO (a) and Fe_2O_3 (b) shrouded ITO tested in 5 mM $K_3[Fe(CN)_6]$ with different scan rates (0.02, 0.05, 0.1, 0.12, 0.15, 0.2, 0.25, 0.3, 0.35, 0.4 V s^{-1}) and their linear relation between the peak reduction current *i* and $s^{1/2}$ obtained via above detections. (c) ECL-potential of ITO with different modification in pH 7.8 PBS (blue, red and green curves refer to pure Au NCs, TAEA/Au NCs and *c*-Fe_2O_3/TAEA/*a*-Au NCs, respectively). (d) CV curves of ITO in the case with or without Fe_2O_3 in 0.01 M TAEA solution. Error bars = SD, (*n* = 3).

RESULTS AND DISCUSSION

Characterization of Fe_2O_3 NAs. The crystallization of Fe_2O_3 is characterized using X-ray diffraction (XRD), and the result is shown in Figure 1a. Multiple distinct diffraction peaks are found at 2θ=24.138°, 33.152°, 35.611°, 40.854°, 54.089°, 63.989° and 75.428°, which correspond to the (012), (104), (110), (113), (116), (300), and (220) planes of Fe_2O_3, respectively.[30] And then, the scanning electron microscopy (SEM) is employed to observe the morphology of the as-synthesized Fe_2O_3 NAs. Figure 1b shows that the purposed Fe_2O_3 is composed of well-ordered nanorods approximately 80 nm in width and 2.5 μm in length with uniformly distributed and highly consistent, which are obtained from the planform and front view (inset), respectively. The above results confirm that the product prepared is indeed Fe_2O_3 NAs.

Characterization of peptide-templated Au NCs. In order to explore the morphologic characters of as-prepared Au NCs, transmission electron microscopy (TEM) images and laser particle size analyzer (LPSA) spectrum are shown in Figure 1c and its inset. As can be seen from that, either TEM or LPSA show uniform particle size of Au NCs about 1.8 ± 0.2 nm with monodisperse distribution. After doubling the magnification of random region, the high-resolution TEM (HRTEM) image of the highly paralleled and ordered lattice fringe with the *d*-spacing of 0.23 nm is observed (Figure 1d and its inset), which is corresponding to the (111) faces of Au NCs well-crystals.[32]

Spectral test, containing circular dichroism (CD) spectrum, UV-vis spectrum, fluorescence emission spectrum and ECL spectrum, are effective indicators to confirm successful as-synthesized Au NCs. The conformation of the polypeptide sequence can change subtly during the period of reaction due to the change of its folding pattern, which can be characterized by the CD spectrum. As can be seen from Figure 2a, the dual characteristic peaks are captured at 219 nm and 198 nm (black curve), which corresponding to the 3_1-helical structure of pure polypeptide without any disposition.[33] Later, the sharp negative peak is redshifted significantly about 200 nm with the disappearance of the broad peak when the reaction is over (red curve), from which is a typical disordered peptide, highlighting the metamorphic conformation of polypeptide in the synthesis process.[33] Additionally, compared with gold nanoparticles, Au NCs should exhibit unique discrete fluorescence under the excitation of ultraviolet illuminant, and since there is no localized surface plasmon resonance, thus no light absorption should occur in the wavelength range from 500 nm to 600 nm, all of the above is well represented in Figure 2b (black and red curves).[34, 35] ECL emission is also a unique indicator for Au NCs evaluation as distinct from nanoparticles.[17] Herein, relatively strong ECL signal with the wavelength of 475 nm (green curve) is detected in the TAEA aqueous solution (10 mL, 0.01 M) by a three-electrode system. The above experimental results are sufficient to prove the successful preparation of Au NCs.

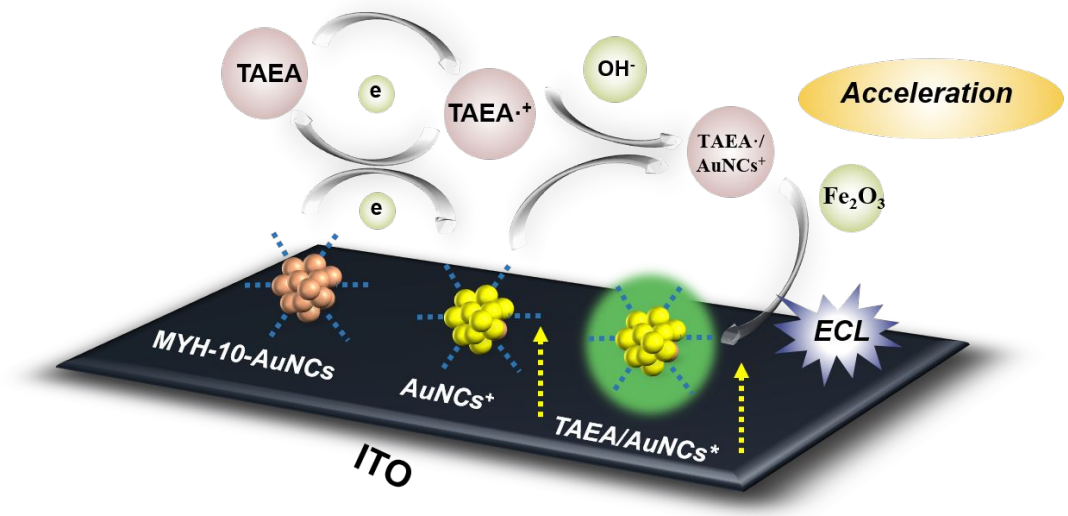

Scheme 2. Possible working mechanism illustration of the enhanced ECL by electrocatalysis.

Verification the bifunctional of MYH-10 polypeptide. The domain B of self-designed polypeptide is a specific antibody capturer, which can effectively recognize the Fc domain to make the antibody fix in a well-ordered mode. To ensure that domain B is not inactivated during synthesis, reversed-phase high performance liquid chromatogram (RP-HPLC) is employed to assess the ability of antibody capture. The single chromatographic peak appeared at 22.2 min with different peak areas when different concentrations of CRFRA 21-1 (2 μg mL^{-1} ~ 12 μg mL^{-1}) are injected into the column (Figure 3a). The obtained calibration curve is expressed as A=37.39+29.47×c exhibited an excellent linearity between the peak area and the concentration of anti-CYFRA21-1 with a high correlation coefficient of 0.996 (inset of Figure 3a). The unconnected amount of antibody are provide in Figure 3b, from which have no visible difference in the antibody recognition of polypeptide before and after synthesis, verifying that MMYY and HFRRHL, two autonomous domains, mutual noninterference.

Increased electro-active surface area of *c*-Fe_2O_3 NAs. It is necessary to demonstrate that the Fe_2O_3 NAs can increase the electro-active surface area, which boost to increase the loading amount of immune molecules. For the purpose, the electro-active surface area of pure ITO and Fe_2O_3 shrouded ITO can be calculated by means of cyclic voltammetry (CV) model utilizing $K_3[Fe(CN)_6]$ as the indicator according to the following equation:[36]

$$i = 2.69\times10^5 AD^{1/2}n^{3/2}v^{1/2}c$$

where i is the independent variable obtained from reductive peak current under different scan rates, A stands for the dependent variable of electro-active surface area (unit of A is cm^2), D is the diffusion coefficient of $K_3[Fe(CN)_6]$ in water medium under room temperature, which is listed as an empirical value of 6.70, n is the electron transfer number of this system, which is assigned as 1 here, v and c refers to the scanning rate the concentration of the electrolyte, respectively. Under different scan rates, the fitted curves of pure ITO and Fe_2O_3 shrouded ITO are obtained as i = 418.80×s+22.67 and i = 427.75×s+48.54 (Figure 4a and b), which correspond to the electro-active surface area of 1.64 cm^{-1} and 3.13 cm^{-1}, respectively. Indeed, the role of Fe_2O_3 NAs is obviously, increasing the electro-active surface area the sensing interface.

ECL performance of *c*-Fe_2O_3/TAEA/*a*-Au NCs. The properties of this ECL system is investigated by the analysis of ECL and CV dates. Three working electrodes with different modified state are detected and the ECL-potential results are shown in Figure 4c. Neither pure Au NCs (530 a.u., blue curve) nor TAEA/Au NCs compound (6900 a.u., red curve) exhibit weak ECL emission, but it is still confirmed that the intramolecular ECL emission of self-enhanced system is endowed with more high ECL efficiency. Nevertheless, the ECL emission of *c*-Fe_2O_3/TAEA/*a*-Au NCs increased significantly to 11349 a.u. (green curve), illustrating that Fe_2O_3 as coreactant accelerator indeed can double the ECL intensity. Otherwise, different oxidation peaks were detected in the case with or without Fe_2O_3 in TAEA solution. It can be clearly seen that the peak shifted negatively from 0.87 V to 0.83 V (Figure 4d), speculating that the interference of Fe_2O_3 alters the free radical reaction.

ECL enhanced mechanism of *c*-Fe_2O_3/TAEA/*a*-Au NCs system. In view of the current situation of ECL signal enhancement, whether is there a synergistic reaction between the ternary system of Au NCs, TAEA and Fe_2O_3, which take on the role of emitter, co-reactant and coreactant accelerator, respectively. As an possible

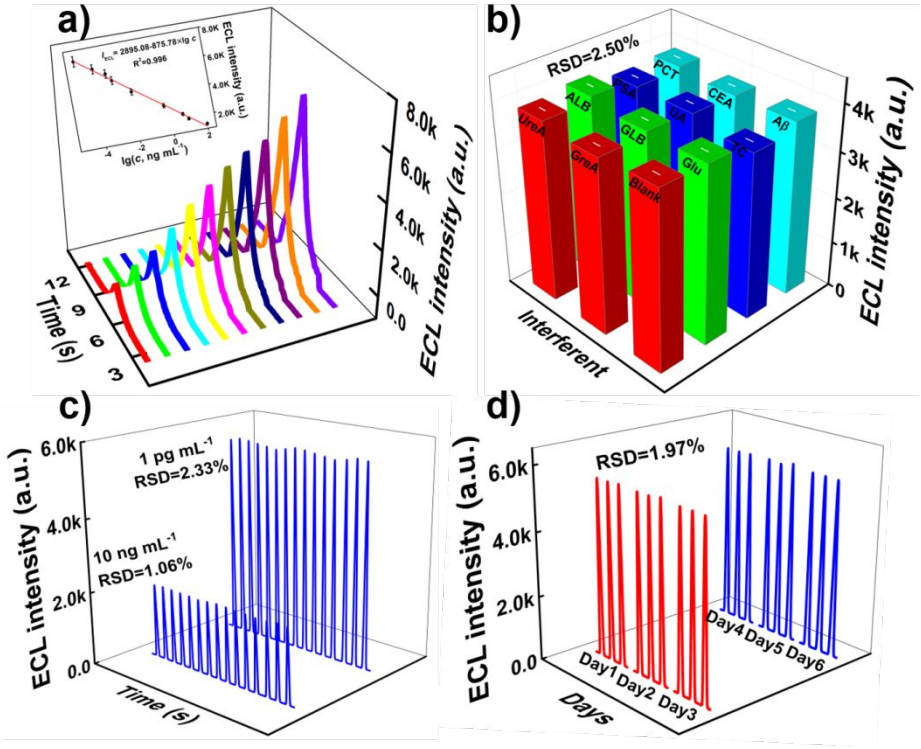

Figure 5. (a) ECL-time curves for CYFRA21-1 with wide concentrations (10 fg mL^{-1} ~ 100 ng mL^{-1}) and calibration curve. (b) Specificity tests of biosensors for 0.1 ng mL^{-1} CYFRA21-1 mix with 0.1 ng mL^{-1}diversified interferent: creatinine (CreA), ureophil (UreA), glutamic acid (Glu), globin (GLB), albumin (ALB), cholesterol (TC), uric acid (UA), prostate-specific antigen (PSA), β-amyloid protein (Aβ), carcino-embryonic antigen (CEA), procalcitonin (PCT). Stability tests of biosensors containing (c) excitation stability under different concentrations and (d) endurance stability by shelving for 1 ~ 6 days. Error bars = SD, (n = 3).

illustration shown in Scheme 2, with the deepening of anode scanning from 0.3 V to 1.2 V, the TAEA/Au NCs conjugate lose electrons to generate radical intermediate of TAEA•$^{+}$/Au NCs^{+} (equation 1). In an alkaline environment, the TAEA•$^{+}$ can form proton state TAEA•/Au NCs^{+} (equation 2), which can occur free radical reaction to form more high-energy-state TAEA/Au NCs* in intramolecular using Fe_2O_3 as accelerator for promotion of electron transfer and energy transmission (equation 3). In the final process, TAEA/Au NCs* return to the ground-state is accompanied by the release of photons (equation 4).[37, 38]

$$\text{TAEA/Au NCs} - 2e \rightarrow \text{TAEA}\bullet^{+}\text{/Au NCs}^{+} \quad (1)$$

$$\text{OH}^{-} + \text{TAEA}\bullet^{+}\text{/Au NCs}^{+} \rightarrow \text{TAEA}\bullet\text{/Au NCs}^{+} \quad (2)$$

$$\text{TAEA}\bullet\text{/Au NCs}^{+} + Fe_2O_3 \rightarrow \text{TAEA/Au NCs}^{*} \quad (3)$$

$$\text{TAEA/Au NCs}^{*} \rightarrow \text{TAEA/Au NCs} + h\nu \quad (4)$$

Utility analysis of as-fabricated biosensor. Compared with sandwich-type biosensors with signal labels, label-free sensors have higher requirements on the performance of signal transducers and the sensing substance, which is the essential reason why they are not be popular. Nevertheless, it would not be negative to develop due to its unique superiority of simple construction process and simplified layering, which is the premise of portability and commercialization. To evaluate the sensing strategies purposed by us, corresponding evaluation methods should be included such as linear dependence towards to target, specificity and stability of sensing platform and real sample analysis.

Under optimal ECL conditions (the detailed analysis are presented in the Supporting Information), the quantitative analysis of CYFRA21-1 are fulfilled using the purposed biosensor (Figure 5a). The obtained calibration curve is expressed as I_{ECL}=2895.08-875.78×lg c (unit of c is ng mL^{-1}) exhibited an excellent linearity between the ECL intensity and the logarithm of CYFRA21-1 concentrations in the range of 10 fg mL^{-1} to 100 ng mL^{-1} (the correlation coefficient is 0.996), as depicted in inset of Figure 5a. By calculation, an unprecedented limit of detection is obtained about 1.33 fg mL^{-1} (S/N=3), which is much lower than other reports.[39-44] The results show that the biosensor has excellent performance in the experimental conditions at least, and fully meets the needs of clinical detection. But, in consideration of the complexity of serum samples, eleven common elements in serum are chosen as interferent mixed

with 0.1 ng mL^{-1} CYFRA21-1 and modified on the electrode surface as targets for specificity evaluation, in which the relative standard deviation (RSD) is 2.50%, revealing the excellent specificity (Figure 5b).

As is known to all, commercial detectors are stored in hospitals, pharmacies and other medical institutions in the period from the factory to the use. This long shelf life is benefit from the high performance of sensing parts and exquisite technology. Take these into account, the stability tests of biosensors are performed. Figure 5c shows the ECL-time curves for 250 s of cyclic excitation of targets CYFRA21-1 with 1 pg mL^{-1} and 10 ng mL^{-1}. Under such long excitation cycle, the ECL signals do not float significantly and the RSDs are 2.33% and 1.06%, respectively. Otherwise, endurance stability is tested by shelving the fabricated biosensor for 1~ 6 days. The three-dimensional diagram shown in Figure 5d of this experiment confirms that the signal intensity will not be disturbed (RSD = 1.97%), indicating good stability of the designed sensors. It is well known that productized detection tools must have ultrahigh reproducibility, for which we used 1 pg mL^{-1} CYFRA21-1 as the target to evaluate the reproducibility of the purposed sensor. As shown in Figure S4, the ECL intensity of nine biosensors varied slightly with a low RSD of 1.47%, which confirmed the good repeatability of the biosensor.

Since real sample analysis can evaluate clinical accuracy and practicality of biosensors, the standard addition method is employed to complete relevant detection. The school hospital provides serum with 0.7 ng mL^{-1} of CYFRA21-1 roots in healthy students (with consent by himself). And then, different concentrations CYFRA21-1 (0.01 ng mL^{-1}, 0.1 ng mL^{-1}, 1 ng mL^{-1}, 10 ng mL^{-1} and 30 ng mL^{-1}) are added above serum and the mixture modified on the electrode as target. All amount found and recoveries are gathered in Table 1, from which the recovery rate is calculated with an unprecedented range from 90.0 to 99.9% (RSD less than 1.03, n=3), revealing that the potential applications of the sensing platform in clinical analysis can be expected.

Table 1. Standard addition data of purposed biosensor for CYFRA21-1 detection.

Simple order	Orign numer (ng mL^{-1})	Spiked samples (ng mL^{-1})	Amount found (ng mL^{-1})	RSD (%,n=3)	Recovery (%)
1		0.01	0. 709	0.38	90.0
2		0.1	0.793	0.59	93.0
3	0.7	1	1.699	0.65	99.9
4		10	10.691	0.26	99.9
5		30	30.664	1.03	99.8

CONCLUSIONS

In summary, MYH-10-biomineralized Au NCs is employed to construct a novel sensing interface for CYFRA21-1 detection. Relevant experiments confirm that MMYY and HFRRHL, two autonomous domains, mutual noninterference. In the synthesis process, the specific antibody capturer HFRRHL hexapeptide can maintain bioactivity completely. The expansion of the bioconjugate to ECL-based biosensor effectively reduces the spatial hindrance of the sensing interface compared with the traditional electrode modification. Combine with intramolecular ECL excitation and co-reaction acceleration strategy using Fe_2O_3 NAs as well-ordered electronic transporter, the ECL intensity of Au NCs can double to meet the requirement of trace analysis.

ASSOCIATED CONTENT

Supporting Information

Materials and regents, apparatus, RP-HPLC analysis for MYH-10 evaluation, ECL detection of purposed biosensor, EIS characterization of stepwise biosensor fabrication, characterization of successful carboxylation of Fe_2O_3 NAs, optimal conditions of the ECL system, repeatability tests of the biosensor

AUTHOR INFORMATION

Corresponding Author

*E-mail: chem_renx@163.com (X. R.);

sdjndxwq@163.com (Q.W.)

Notes

The authors declare no competing financial interest.

ACKNOWLEDGMENTS

This work was supported by the National Key Scientific Instrument and Equipment Development Project of China (No.21627809); National Natural Science Foundation of China (No. 21777056), Jinan Scientific Research Leader Workshop Project (2018GXRC024), Special Foundation for Taishan Scholar Professorship of Shandong Province.

REFERENCES

1. Yu, H. J.; Zou, Y. L.; Jiang, L.; Yin, Q.; He, X. Y.; Chen, L. L.; Zhang, Z. W.; Gu, W. W.; Li, Y. P., Induction of apoptosis in non-small cell lung cancer by downregulation of MDM2 using pH-responsive PMPC-b-PDPA/siRNA complex nanoparticles. *Biomaterials* **2013,** *34* (11), 2738-2747.

2. Dohmoto, K.; Hojo, S.; Fujita, J.; Yang, Y.; Ueda, Y.; Bandoh, S.; Yamaji, Y.; Ohtsuki, Y.; Dobashi, N.; Ishida, T.; Takahara, J., The role of caspase 3 in producing cytokeratin 19 fragment (CYFRA21-1) in human lung cancer cell lines. *Int. J. Cancer* **2001,** *91* (4), 468-473.

3. Kim, K. R.; Kim, H. J.; Hong, J. I., Electrogenerated Chemiluminescent Chemodosimeter Based on a Cyclometalated Iridium(III) Complex for Sensitive Detection of Thiophenol. *Anal. Chem.* **2019,** *91* (2), 1353-1359.

4. Makaraviciute, A.; Ramanaviciene, A., Site-directed antibody immobilization techniques for immunosensors. *Biosens Bioelectron* **2013,** *50*, 460-471.

5. Yang, L.; Li, Y. Y.; Zhang, Y.; Fan, D. W.; Pang, X. H.; Wei, Q.; Du, B., 3D Nanostructured Palladium-Functionalized Graphene-Aerogel-Supported Fe3O4 for Enhanced $Ru(bpy)_3^{2+}$-Based Electrochemiluminescent Immunosensing of Prostate Specific Antigen. *ACS Appl. Mater. Interfaces* **2017,** *9* (40), 35260-35267.

6. Dong, X.; Zhao, G. H.; Liu, L.; Li, X.; Wei, Q.; Cao, W., Ultrasensitive competitive method-based electrochemiluminescence immunosensor for diethylstilbestrol detection based on $Ru(bpy)_3^{2+}$ as luminophor encapsulated in metal organic frameworks UiO-67. *Biosens. Bioelectron.* **2018,** *110*, 201-206.

7. Choi, S.; Larrain, F. A.; Wang, C. Y.; Fuentes-Hernandez, C.; Chou, W. F.; Kippelen, B., Self-forming electrode modification in organic field-effect transistors. *J. Mater. Chem. C* **2016,** *4* (35), 8297-8303.

8. Dietrich, H. R. C.; Knoll, J.; van den Doel, L. R.; van Dedem, G. W. K.; Daran-Lapujade, P. A. S.; van Vliet, L. J.; Moerman, R.; Pronk, J. T.; Young, I. T., Nanoarrays: A method for performing enzymatic assays. *Anal. Chem.* **2004,** *76* (14), 4112-4117.

9. Hou, J. G.; Wu, Y. Z.; Zhang, B.; Cao, S. Y.; Li, Z. W.; Sun, L. C., Rational Design of Nanoarray Architectures for Electrocatalytic Water Splitting. *Adv. Funct. Mater.* **2019,** *29* (20), 39.

10. Han, F. F.; Xu, J.; Zhou, J.; Tang, J.; Tang, W. H., Oxygen vacancy-engineered Fe_2O_3 nanoarrays as free-standing electrodes for flexible asymmetric supercapacitors. *Nanoscale* **2019,** *11* (26), 12477-12483.

11. Luo, Z. B.; Li, C. C.; Liu, S. S.; Wang, T.; Gong, J. L., Gradient doping of phosphorus in Fe_2O_3 nanoarray photoanodes for enhanced charge separation. *Chem. Sci.* **2017,** *8* (1), 91-100.

12. Ma, M. N.; Zhuo, Y.; Yuan, R.; Chai, Y. Q., New Signal Amplification Strategy Using Semicarbazide as Co-reaction Accelerator for Highly Sensitive Electrochemiluminescent Aptasensor Construction. *Anal. Chem.* **2015,** *87* (22), 11389-11397.

13. Al-Kutubi, H.; Voci, S.; Rassaei, L.; Sojic, N.; Mathwig, K., Enhanced annihilation electrochemiluminescence by nanofluidic confinement. *Chem. Sci.* **2018,** *9* (48), 8946-8950.

14. Lei, Y. M.; Zhuo, Y.; Guo, M. L.; Chai, Y. Q.; Yuan, R., Pore Confinement-Enhanced Electrochemiluminescence on SnO_2 Nanocrystal Xerogel with NO^{3-} As Co-Reactant and Its Application in Facile and Sensitive Bioanalysis. *Anal. Chem.* **2020,** *92* (3), 2839-2846.

15. Miao, W.; Choi, J.-P.; Bard, A. J., Electrogenerated chemiluminescence 69: the tris(2,2'-bipyridine)ruthenium(II), $Ru(bpy)_3^{2+}$/tri-n-propylamine (TPrA) system revisited-a new route involving $TPrA^{*+}$ cation radicals. *J. Am. Chem. Soc.* **2002,** *124* (48), 14478-14485.

16. Wang, T. Y.; Wang, D. C.; Padelford, J. W.; Jiang, J.; Wang, G. L., Near-Infrared Electrogenerated Chemiluminescence from Aqueous Soluble Lipoic Acid Au Nanoclusters. *J. Am. Chem. Soc.* **2016,** *138* (20), 6380-6383.

17. Zhou, Y.; Chen, S.; Luo, X.; Chai, Y.; Yuan, R., Ternary Electrochemiluminescence Nanostructure of Au Nanoclusters as a Highly Efficient Signal Label for Ultrasensitive Detection of Cancer Biomarkers. *Anal. Chem.* **2018,** *90* (16), 10024-10030.

18. Yang, L.; Jia, Y.; Wu, D.; Zhang, Y.; Ju, H. X.; Du, Y.; Ma, H. M.; Wei, Q., Synthesis and Application of CeO_2/SnS_2 Heterostructures as a Highly Efficient Coreaction Accelerator in the Luminol-Dissolved O_2 System for Ultrasensitive Biomarkers Immunoassay. *Anal. Chem.* **2019,** *91* (21), 14066-14073.

19. Zhao, M.; Chen, A. Y.; Huang, D.; Chai, Y. Q.; Zhuo, Y.; Yuan, R., MoS_2 Quantum Dots as New Electrochemiluminescence Emitters for Ultrasensitive Bioanalysis of Lipopolysaccharide. *Anal. Chem.* **2017,** *89* (16), 8335-8342.

20. Bruce, D.; Richter, M. M., Green electrochemiluminescence from ortho-metalated tris(2-phenylpyridine)iridium(III). *Anal. Chem.* **2002,** *74* (6), 1340-1342.

21. Li, L. L.; Liu, H. Y.; Shen, Y. Y.; Zhang, J. R.; Zhu, J. J., Electrogenerated Chemiluminescence of Au Nanoclusters for the Detection of Dopamine. *Anal. Chem.* **2011,** *83* (3), 661-665.

22. Fang, Y. M.; Song, J.; Li, J. A.; Wang, Y. W.; Yang, H. H.; Sun, J. J.; Chen, G. N., Electrogenerated chemiluminescence from Au nanoclusters. *Chem. Commun.* **2011,** *47* (8), 2369-2371.

23. Tan, Y. N.; Lee, J. Y.; Wang, D. I. C., Uncovering the Design Rules for Peptide Synthesis of Metal Nanoparticles. *J. Am. Chem. Soc.* **2010,** *132* (16), 5677-5686.

24. Cui, Y. Y.; Wang, Y. L.; Liu, R.; Sun, Z. P.; Wei, Y. T.; Zhao, Y. L.; Gao, X. Y., Serial Silver Clusters Biomineralized by One Peptide. *ACS Nano* **2011,** *5* (11), 8684-8689.

25. Wang, Y. L.; Cui, Y. Y.; Zhao, Y. L.; Liu, R.; Sun, Z. P.; Li, W.; Gao, X. Y., Bifunctional peptides that precisely biomineralize Au clusters and specifically stain cell nuclei. *Chem. Commun.* **2012,** *48* (6), 871-873.

26. Naik, R. R.; Stringer, S. J.; Agarwal, G.; Jones, S. E.; Stone, M. O., Biomimetic synthesis and patterning of silver nanoparticles. *Nat. Mater.* **2002,** *1* (3), 169-172.

27. Xie, J. P.; Lee, J. Y.; Wang, D. I. C.; Ting, Y. P., Silver nanoplates: From biological to biomimetic synthesis. *ACS Nano* **2007,** *1* (5), 429-439.

28. Naik, A. D.; Menegatti, S.; Gurgel, P. V.; Carbonell, R. G., Performance of hexamer peptide ligands for affinity purification of immunoglobulin G from commercial cell culture media. *J. Chromatogr. A* **2011,** *1218* (13), 1691-1700.

29. Liu, Z.; Gurgel, P. V.; Carbonell, R. G., Effects of peptide density and elution pH on affinity chromatographic purification of human immunoglobulins A and M. *J. Chromatogr. A* **2011,** *1218* (46), 8344-8352.

30. Zhang, R.; Yang, L.; Huang, X. N.; Chen, T.; Qu, F. L.; Liu, Z.; Du, G.; Asiri, A. M.; Sun, X. P., Se doping: an effective strategy toward Fe_2O_3 nanorod arrays for greatly enhanced solar water oxidation. *J. Mater. Chem. A* **2017,** *5* (24), 12086-12090.

31. Zhou, H.; Han, T. Q.; Wei, Q.; Zhang, S. S., Efficient Enhancement of Electrochemiluminescence from Cadmium Sulfide Quantum Dots by Glucose Oxidase Mimicking Gold Nanoparticles for Highly Sensitive Assay of Methyltransferase Activity. *Anal. Chem.* **2016,** *88* (5), 2976-2983.

32. Xie, J.; Zheng, Y.; Ying, J. Y., Protein-directed synthesis of highly fluorescent gold nanoclusters. *J. Am. Chem. Soc.* **2009,** *131* (3), 888-889.

33. Ruzza, P.; Calderan, A.; Guiotto, A.; Osler, A.; Borin, G., Tat cell-penetrating peptide has the characteristics of a poly(proline) II helix in aqueous solution and in SDS micelles. *J. Pept. Sci.* **2004,** *10* (7), 423-426.

34. Zhang, C.; Fan, Y.; Zhang, H.; Chen, S. H.; Yuan, R., An ultrasensitive signal-on electrochemiluminescence biosensor based on Au nanoclusters for detecting acetylthiocholine. *Anal. Bioanal. Chem.* **2019,** *411* (4), 905-913.

35. Grabar, K. C.; Brown, K. R.; Keating, C. D.; Stranick, S. J.; Tang, S. L.; Natan, M. J., Nanoscale characterization of gold colloid monolayers: a comparison of four techniques. *Anal. Chem.* **1997,** *69* (3), 471-477.

36. Li, L. L.; Liu, K. P.; Yang, G. H.; Wang, C. M.; Zhang, J. R.; Zhu, J. J., Fabrication of Graphene-Quantum Dots Composites for Sensitive Electrogenerated Chemiluminescence Immunosensing. *Adv. Funct. Mater.* **2011,** *21* (5), 869-878.

37. Yue, X. X.; Zhu, Z. Y.; Zhang, M. N.; Ye, Z. Q., Reaction-Based Turn-on Electrochemiluminescent Sensor with a Ruthenium(II) Complex for Selective Detection of Extracellular Hydrogen Sulfide in Rat Brain. *Anal. Chem.* **2015,** *87* (3), 1839-1845.

38. Zu, Y. B.; Bard, A. J., Electrogenerated chemiluminescence. 66. The role of direct coreactant oxidation in the ruthenium tris(2,2')bipyridyl/tripropylamine system and the effect of halide ions on the emission intensity. *Anal. Chem.* **2000,** *72* (14), 3223-3232.

39. Zhao, L. H.; Han, H. L.; Ma, Z. F., Improved screen-printed carbon electrode for multiplexed label-free amperometric immuniosensor: Addressing its conductivity and reproducibility challenges. *Biosens. Bioelectron.* **2018,** *101*, 304-310.

40. Yu, Y. Y.; Huang, Z. N.; Zhou, Y.; Zhang, L. H.; Liu, A. L.; Chen, W.; Lin, J. H.; Peng, H. P., Facile and highly sensitive photoelectrochemical biosensing platform based on hierarchical architectured polydopamine/tungsten oxide nanocomposite film. *Biosens. Bioelectron.* **2019,** *126*, 1-6.

41. Chen, Z. H.; Liang, R. L.; Guo, X. X.; Liang, J. Y.; Deng, Q. T.; Li, M.; An, T. X.; Liu, T. C.; Wu, Y. S., Simultaneous quantitation of cytokeratin-19 fragment and carcinoembryonic antigen in human serum via quantum dot-doped nanoparticles. *Biosens. Bioelectron.* **2017,** *91*, 60-65.

42. Kumar, S.; Sharma, J. G.; Maji, S.; Malhotra, B. D., Nanostructured zirconia decorated reduced graphene oxide based efficient biosensing platform for non-invasive oral cancer detection. *Biosens. Bioelectron.* **2016,** *78*, 497-504.

43. Zeng, Y.; Bao, J.; Zhao, Y. N.; Huo, D. Q.; Chen, M.; Yang, M.; Fa, H. B.; Hou, C. J., A sensitive label-free electrochemical immunosensor for detection of cytokeratin 19 fragment antigen 21-1 based on 3D graphene with gold nanopaticle modified electrode. *Talanta* **2018,** *178*, 122-128.

44. Pachauri, N.; Dave, K.; Dinda, A.; Solanki, P. R., Cubic CeO_2 implanted reduced graphene oxide-based highly sensitive biosensor for non-invasive oral cancer biomarker detection. *J. Mat. Chem. B* **2018,** *6* (19), 3000-3012.

For TOC graphic only: